nature geoscience

Article

https://doi.org/10.1038/s41561-022-01095-x

Early Pleistocene East Antarctic temperature in phase with local insolation

Received: 19 April 2022

Accepted: 26 October 2022

Published online: 08 December 2022

Check for updates

Yuzhen Yan[1], Andrei V. Kurbatov[2,3], Paul A. Mayewski[2], Sarah Shackleton[1] & John A. Higgins[1]

Pleistocene glacial–interglacial cycles are hypothesized to be modulated by Earth's orbital parameters through their influence on the Northern Hemisphere summer insolation. Changes in obliquity—Earth's axial tilt—can explain the 41,000-year glacial cycles in the Early Pleistocene. However, the absence of 19,000- and 23,000-year frequencies corresponding to Earth's precession of the rotation axis from those cycles remains enigmatic. Here we investigate how these orbital forcings may have changed by developing an insolation proxy based on the oxygen-to-nitrogen ratio of gases trapped in ice core samples collected from the Allan Hills Blue Ice Area in East Antarctica. We find that East Antarctic temperature was positively correlated with local, Southern Hemisphere summer insolation in the Early Pleistocene, while this correlation became negative in the late Pleistocene, with only the latter being consistent with the previous findings that Northern Hemisphere insolation paced Antarctic climate. If Early Pleistocene ice volume and local Antarctic temperature co-varied, our result supports the hypothesis that attributes the absence of precession in the 41,000-year glacial cycles to cancellation of precession frequencies in hemispheric ice volume changes that are responding to local insolation, suggesting a more dynamic East Antarctic Ice Sheet in the Early Pleistocene than in the past 800,000 years.

During the Pleistocene Epoch (2.58 million years ago (Ma) to 11.7 thousand years ago (ka)), intervals with extensive continental glaciation in the Americas and Eurasia (glacial) alternated with intervals in which large ice sheets were restricted to Greenland and Antarctica (interglacial). These glacial cycles are captured by the isotopic composition of oxygen ($\delta^{18}O$) in benthic foraminifera, a classic proxy for ice volume and seawater temperature[1–3]. The δ notation here is expressed as $R_{sample} / R_{standard} - 1$, where R is the ratio of interest. Before approximately 1.2 Ma, the benthic $\delta^{18}O$ time series has a 41 thousand year (kyr) period, often interpreted to reflect insolation forcing driven by variations of Earth's axial tilt (obliquity)[1]. After approximately 0.7 Ma, glacial cycles lengthened to an irregular, asymmetrical, but roughly approximately 100 kyr period, numerically compatible with the eccentricity variability of Earth's orbit. The shift from the 41 kyr to the quasi-100 kyr cycle between approximately 1.2 Ma and 0.7 Ma is known as the Mid-Pleistocene Transition (MPT)[4].

An enigma in the Early Pleistocene 41 kyr glacial cycles is the very weak expression of precession-related periods in the global $\delta^{18}O$ records, despite clear and strong 23 kyr cycles in insolation[5]. This conundrum, colloquially known as 'the 40 kyr problem', has been explained in two ways. One hypothesis[6,7] points to the 65° N integrated summer insolation (ISI) above 275 W m^{-2}, whose power spectrum has little periodicity related to precession due to Kepler's second law: when precession places the warmest boreal summer at perihelion, its duration is also the shortest. A competing hypothesis[8,9] invokes a dynamic East Antarctic Ice Sheet (EAIS) responding to local summer insolation. Because precession forcing is out of phase between the Northern and Southern hemispheres, precession-related cycles would be suppressed

[1]Department of Geosciences, Princeton University, Princeton, NJ, USA. [2]Climate Change Institute, University of Maine, Orono, ME, USA. [3]School of Earth and Climate Sciences, University of Maine, Orono, ME, USA. e-mail: yanyuzhen.pku@gmail.com

in the globally averaged oxygen isotope record but would still exist in local records specific to one hemisphere.

Testing theses hypotheses remains challenging in part due to a dearth of polar climate records dating back to the Early Pleistocene, particularly from the Southern Hemisphere. In addition, where such records exist, insolation rarely leaves a direct imprint in geologic records and instead needs to be calculated from the chronology, which is often based on orbital tuning (thus constituting a circular logic). Even when the timescale is established by independent age control points, precession-related cycles are not fully resolved because of the low temporal resolution of the records[10] or the limited number of those individual age control points[11–13].

Ice cores offer a different perspective to address the '40 kyr problem' because insolation leaves a direct fingerprint in the ice (next section). Moreover, a dynamic EAIS response to local insolation in the Early Pleistocene hypothesized by ref. [8] implies that East Antarctic temperature would also be paced by local summer insolation (with a delayed response) unless the Antarctic ice volume is completely de-coupled from local climate on orbital frequencies, a possibility we cannot fully rule out. Nonetheless, Late Pleistocene global ice volume has been tightly coupled with Antarctic temperature[14,15], possibly via ice sheet elevation changes and/or the dependence of ablation on summer temperature[8]. In turn, Antarctic temperature was paced by Northern Hemisphere summer insolation[16–18] (or Southern Hemisphere summer duration[19]) in the late Pleistocene. Therefore, although definitive evidence to conclusively establish the ice volume–Antarctic temperature relationship is missing, we assume a continued connection between Antarctic ice volume and temperature. An ice core approach to address the '40 kyr problem' is thus (1) finding ice dating back to the Early Pleistocene, (2) retrieving insolation signals and (3) comparing the insolation signals with temperature proxies.

Stratigraphically discontinuous ice cores dating back to 1.5 Ma and 2.0 Ma have recently been recovered from the Allan Hills Blue Ice Area, East Antarctica, providing 'climate snapshots' extending well into the Early Pleistocene[20]. Allan Hills is a nunatak, the extruded portion of a subglacial topographic barrier. It guides the glacial flow towards the surface[21,22], where ablation by katabatic wind maintains local ice mass balance and leads to the formation of exhumed crystalline ice. Absolute ages of the ice were determined from the triple argon isotope composition ($^{40}Ar_{atm}$; Methods and refs. [20,23,24]) without any presumed connections to orbital parameters. We acknowledge that the analytical uncertainties of the $^{40}Ar_{atm}$ measurements are at least 10% of the sample age, thus preventing the establishment of a precise time series. While it might seem that without a precise chronology, the insolation values cannot be accurately calculated, our approach takes advantage of the imprint of insolation preserved in the ice and does not require the record to be continuous, as explained below.

Insolation imprint in Antarctic ice

O_2/N_2 (as $\delta O_2/N_2$) and Ar/N_2 (as $\delta Ar/N_2$) ratios of the trapped air in ice cores are utilized as a proxy for insolation intensity during local summer solstice. We compiled previously published Dome C[18,25–27], Dome Fuji[16,28], Vostok[29] and Allan Hills[30,31] $\delta O_2/N_2$ data and corrected the data for (1) gravitational fractionation using the $\delta^{15}N$ of N_2 (ref. [32]), (2) the long-term decline in the atmospheric O_2 concentration (PO_2) in the Late Pleistocene[31,33] and (3) where applicable, the decrease in modern PO_2 due to combustion of fossil fuels[34] (Methods and Extended Data Table 1). Over the past 800 kyr, the $\delta O_2/N_2$ and $\delta Ar/N_2$ of trapped gases covary (Extended Data Fig. 1), so do these ratios and the local summer insolation (Fig. 1 and Extended Data Figs. 2 and 3). The hypothesized root of these correlations is that the intensity of sunlight on the surface of the ice sheet determines the extent and nature of snow metamorphism, which in turn modulates the magnitude of O_2 and Ar losses relative to N_2 at the 'bubble close-off depth' (typically 70–120 m in polar regions)[29,35].

Normally, air is trapped at the close-off depth and thus younger than the enclosing ice. However, the ice grain properties that influence $\delta O_2/N_2$ are set at the surface. As a result, the age of merit for gas ratios is the ice age rather than the gas age[29,35]. $\delta O_2/N_2$ and $\delta Ar/N_2$ ratios in the trapped air are therefore ideal insolation proxies to examine the relationship between insolation and Antarctic temperature, which can be estimated by the stable isotope composition of ice (such as deuterium, expressed as δD_{ice}, or ^{18}O, as $\delta^{18}O_{ice}$)[36]. Because insolation and δD_{ice} are registered in the same depth, evaluating their connections is not predicated upon an intact stratigraphy. We caution that δD_{ice} is also sensitive to additional factors such as moisture source conditions[37] and sea ice[38], which cannot be completely ruled out in the case of Allan Hills samples. Nevertheless, over the past seven glacial cycles, δD_{ice} of one East Antarctic ice core is observed to correlate well with the site temperature (based on corrections to δD_{ice} by deuterium excess) on orbital and even millennial timescales[39], so we assume δD_{ice} as a primary temperature proxy.

Another valid concern of this approach arises from the observation that the correlation between $\delta O_2/N_2$ and insolation is stronger in some cores than in others (Fig. 1). Additional processes likely also affect the gas ratios, such as the secondary influence on the gas ratios by accumulation rates on multidecadal timescales[40]. For Allan Hills samples greater than 800 ka, $\delta O_2/N_2$ variability on such short timescales should be lost due to diffusive smoothing (Supplementary Information and ref. [41]). If not, the presumed $\delta O_2/N_2$ accumulation rate connection should at least remain stable over time. The other possibility is related to gas preservation, in particular, ice-containing bubbles versus clathrates. Bubbly ice has more intrinsic high-frequency variability in $\delta O_2/N_2$ and is more prone to post-coring gas losses than clathrate ice (Supplementary Figs. 1 and 2). However, such high-frequency variabilities are expected to manifest as white noise (Supplementary Information), so a statistically significant correlation with δD_{ice} must arise from insolation or accumulation rates.

Antarctic climate link to insolation

Before examining the relationship between $\delta O_2/N_2$ (insolation) and δD_{ice} (temperature) in the ice, we describe the attribution of ages to the Allan Hills $\delta O_2/N_2$ samples dating to the Early Pleistocene here because they were measured on sections different from those used for $^{40}Ar_{atm}$ dating. A full description can be found in Yan et al.[31]. In brief, each $\delta O_2/N_2$ sample was assigned the age of the closest $^{40}Ar_{atm}$ sample. Next, we binned samples into the four dominant age groups and calculated the average of $^{40}Ar_{atm}$ ages weighted by their respective analytical uncertainty. The four time slices reported in the present study are: 400 ka (± 70 ka), 810 ka (± 100 ka), 1.5 Ma (± 0.1 Ma) and 2.0 Ma (± 0.1 Ma). Numbers in brackets are the ± 95% confidence intervals (CIs) of the age bin constrained by the analytical uncertainties of individual measurements and do not necessarily reflect the true spread of the data. To complement the temporal coverages of Early Pleistocene glacial cycles, the 2.0 Ma age bin (sample number $N = 4$) excluded in Yan et al.[31] is retained in this work (Methods).

When δD_{ice} is plotted against $\delta O_2/N_2$ measured in ice from the same depth (Fig. 2), $\delta O_2/N_2$ is negatively correlated with δD_{ice} in 1.5 Ma and 2.0 Ma Allan Hills samples at a significance level of 0.05 ($N = 29$; $r = -0.539$; two-tailed $p < 0.01$). We note that excluding the four 2.0 Ma data points, a negative correlation between $\delta O_2/N_2$ and δD_{ice} in the 1.5 Ma samples persists, but this correlation is no longer statistically significant (two-tailed $p = 0.06$; Extended Data Fig. 4) due to a smaller sample size. In samples dating to and after the MPT, however, $\delta O_2/N_2$ and δD_{ice} are positively correlated (although the correlation is not significant in the Late Pleistocene samples from the Allan Hills). $\delta Ar/N_2$ exhibits a similar relationship with δD_{ice}: a negative correlation before the MPT ($r = -0.534$; two-tailed $p < 0.05$) and a positive but non-significant correlation afterwards (Extended Data Fig. 5). A positive relationship between $\delta O_2/N_2$ and δD_{ice} is also present in the Dome

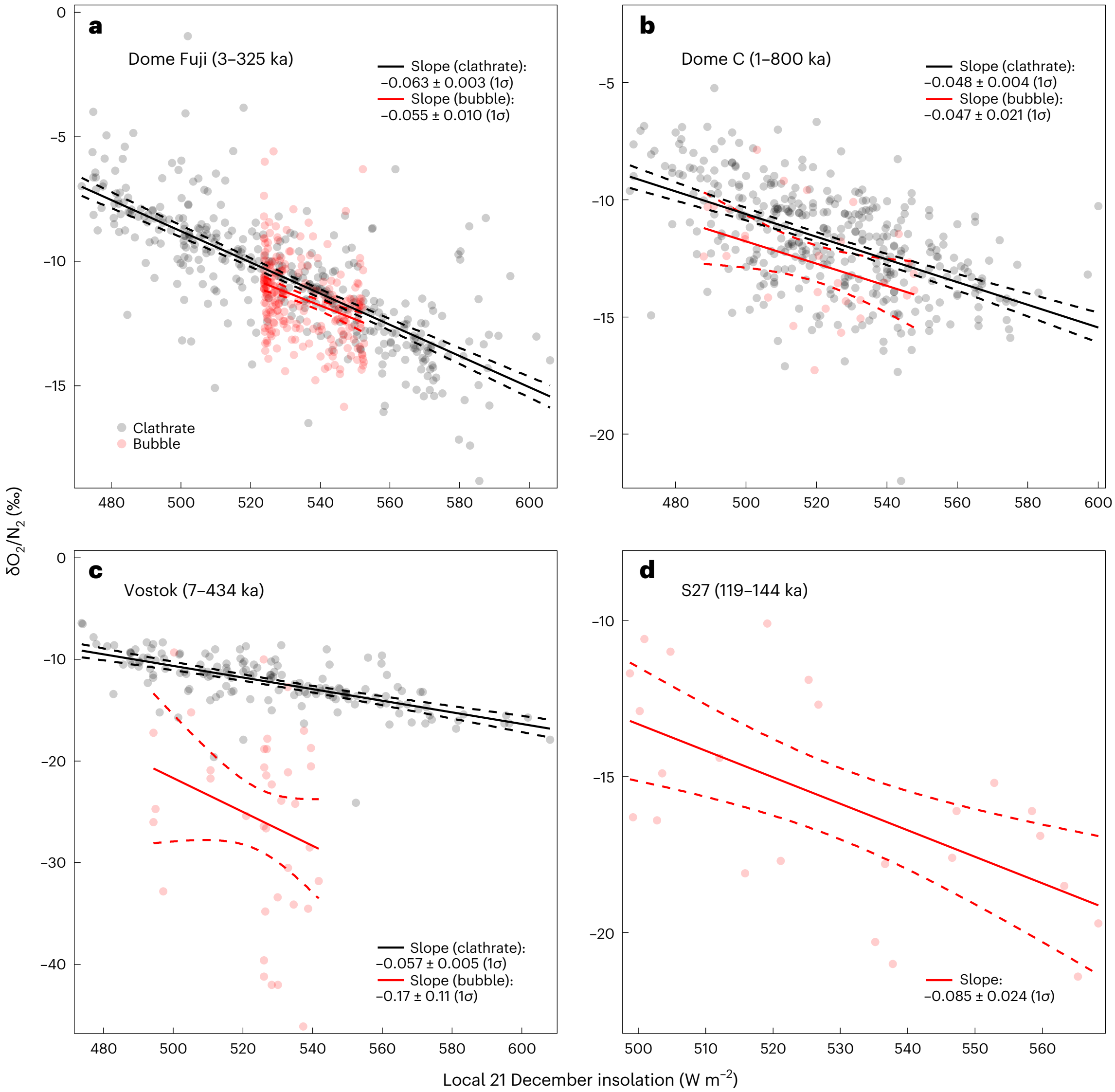

Fig. 1 | $\delta O_2/N_2$ as a proxy for local 21 December insolation intensity observed in four Antarctic ice cores. a, Dome Fuji[16,28]. **b**, Dome C[18,25–27]. **c**, Vostok[29]. **d**, Allan Hills S27 (ref. [30]). $\delta O_2/N_2$ values have been corrected for the Late Pleistocene decline in atmospheric O_2 (ref. [33]) and normalized to the present day. Black circles indicate samples in which gases exist exclusively in the form of clathrate. Clathrate-derived $\delta O_2/N_2$ is significantly ($p < 0.01$) correlated with the insolation intensity at local summer solstice in Dome Fuji (sample $N = 366$, $r^2 = 0.58$), Dome C ($N = 365$, $r^2 = 0.29$) and Vostok ($N = 157$, $r^2 = 0.44$) ice. Two-tailed p values are reported here and below. Red circles indicate samples where gases are trapped in bubbles. The S27 ice has no clathrate in it. The bubble-derived $\delta O_2/N_2$ has a weaker correlation when compared to clathrate-based $\delta O_2/N_2$ but is still significantly correlated with local summer insolation intensity in Dome F ($N = 238$, $r^2 = 0.12$, $p < 0.01$), Dome C ($N = 29$, $r^2 = 0.17$, $p = 0.03$) and S27 ($N = 24$, $r^2 = 0.37$, $p < 0.01$). In Vostok, bubble-based $\delta O_2/N_2$ has anomalously low (<−30‰) values, which could arise from the poor core quality as noted by Bender et al.[29]. Vostok $\delta O_2/N_2$ is not significantly correlated with insolation ($N = 37$, $r^2 = 0.06$, $p = 0.14$). Insolation is calculated from Laskar et al.[47]. Dashed lines represent 95% confidence interval of the linear regression line, with the 1 standard deviation (1σ) reported in each sub-figure.

F, Vostok and Dome C ice record younger than 800 ka (Extended Data Fig. 6). Despite the low correlation coefficient ($r^2 < 0.2$) in these records, time-series analyses reveal the imprint of Northern Hemisphere insolation in those Antarctic δD records[16–18].

The most straightforward interpretation of the negative correlation between δD_{ice} and $\delta O_2/N_2$ is that in the Early Pleistocene, higher summer insolation (lower $\delta O_2/N_2$) was associated with warmer local Allan Hills temperature (higher δD_{ice}). However, whether this correlation will hold in light of analytical uncertainties associated with $\delta O_2/N_2$ and $\delta Ar/N_2$ analyses remains to be tested. We thus performed a Monte Carlo simulation that explicitly includes these uncertainties (Methods) and found a 4% chance that an insignificant δD_{ice}–$\delta O_2/N_2$ correlation arises (Fig. 3). The observed negative correlation is therefore considered robust. Similar Monte Carlo simulations considering the analytical uncertainties in $\delta Ar/N_2$ yield an insignificant correlation with δD_{ice} in 1.5 Ma and 2.0 Ma samples at >5% probability (Extended Data Fig. 5). The less robust correlation between $\delta Ar/N_2$ and δD_{ice} is possibly due to a lower signal-to-noise ratio (that is, insolation versus noise) in $\delta Ar/N_2$ data. In addition, it is possible that Allan Hills represents a climatologically sensitive region in East Antarctica. In this case, this single site does not represent the full continent. We acknowledge this possibility but note that δD_{ice} measured on Allan Hills samples dating between approximately 115 ka and 250 ka show overall good agreement with two other East Antarctic deep ice cores (Talos Dome and Dome C) on orbital timescales[42]. We therefore proceed with interpreting the observed change in the δD_{ice}–$\delta O_2/N_2$ relationship in the context of East Antarctic temperature response to insolation forcing.

 https://doi.org/10.1038/s41561-022-01095-x

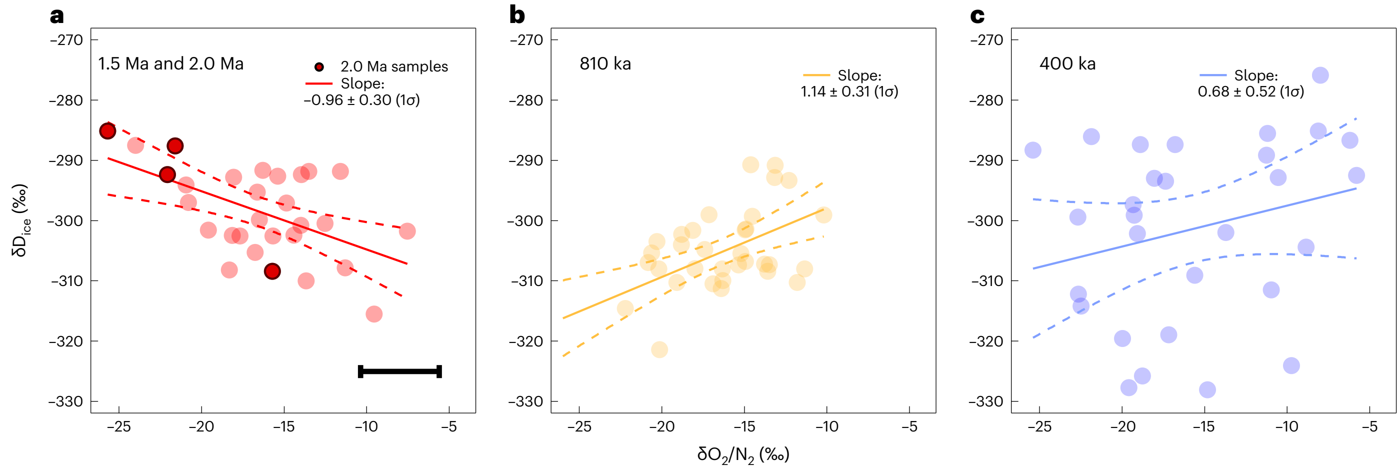

Fig. 2 | Relationship of the isotopic composition of ice (δD_{ice}) and $\delta O_2/N_2$ of the trapped air in the Allan Hills blue ice. a, 1.5 Ma and 2.0 Ma (sample $N = 29$, $r^2 = 0.29$, two-tailed $p < 0.01$), where the four 2.0 Ma samples are shown in dark red. **b**, 810 ka ($N = 34$, $r^2 = 0.30$, $p < 0.01$). **c**, 400 ka samples ($N = 29$, $r^2 = 0.06$, $p = 0.19$). The horizontal error bar in **a** represents the pooled standard error of the $\delta O_2/N_2$ measurements (± 2.38 ‰). Dashed lines represent 95% confidence interval. Note that the three panels have the same scale of *x* and *y* axes to demonstrate that $\delta O_2/N_2$ data have similar range in all three intervals, but δD_{ice} variabilities are larger in the Late Pleistocene.

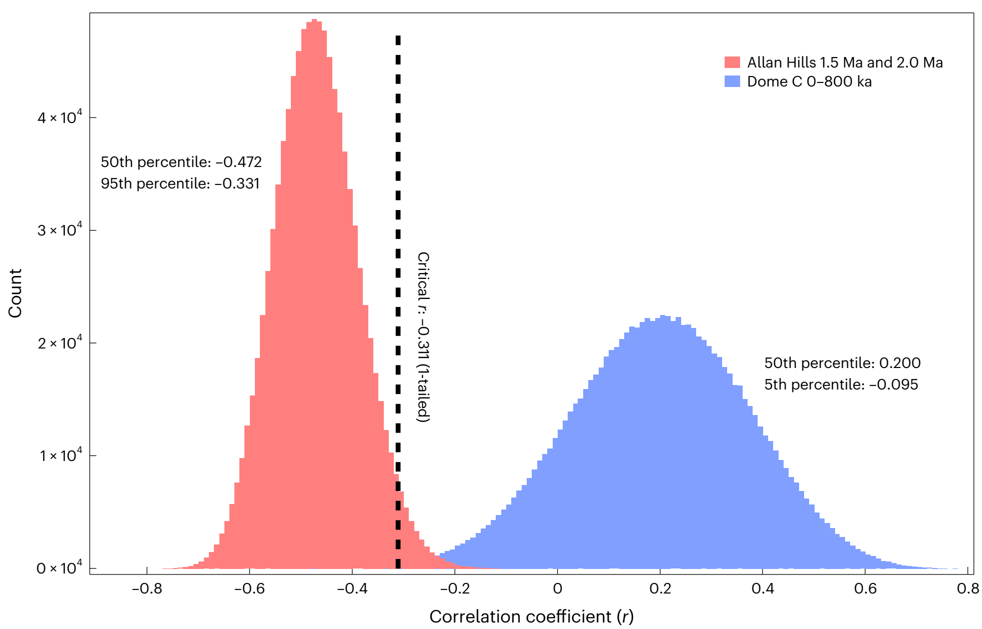

Fig. 3 | Testing the statistical robustness of and the alternative explanation of Northern Hemisphere pacing for the observed negative δD_{ice}–$\delta O_2/N_2$ relationship in the 1.5 Ma and 2.0 Ma Allan Hills samples. Red bars: distribution of the correlation coefficient *r* between 29 pairs of δD_{ice} and $\delta O_2/N_2$ in 1.5 Ma and 2.0 Ma samples. In each of the 10^6 iterations, the analytical uncertainties of $\delta O_2/N_2$ measurements are explicitly considered and propagated into the synthetic series (Methods). Blue bars: distribution of the correlation coefficient *r* between 29 randomly selected δD_{ice} and $\delta O_2/N_2$ data points from the continuous 800 kyr Dome C record. 10^6 iterations were performed. Histogram bin width is 0.01.

Implications for glacial cycles

Now we ask if the observed negative correlation between $\delta O_2/N_2$ and δD_{ice} could be explained by hypotheses other than the direct pacing of Antarctic temperature by local insolation in the Early Pleistocene.

First, consider the hypothesis that Pleistocene Antarctic temperature has always been paced by Northern Hemisphere insolation. The negative correlation between $\delta O_2/N_2$ and δD_{ice} could fortuitously arise if the discontinuous blue ice happens to record an interval with only obliquity-driven changes (for example, when eccentricity is low), which the $^{40}Ar_{atm}$ measurements cannot resolve. This scenario is unlikely because the range of $\delta O_2/N_2$ data is similar in the 1.5 Ma and 2.0 Ma samples compared with that in the Late Pleistocene data (Extended Data Fig. 7), and the δD_{ice} in the 1.5 Ma and 2.0 Ma ice spans roughly half the range of δD_{ice} observed in a Late Pleistocene glacial cycle[20]. Even if the ice covers both precession and obliquity cycles, discrete sampling by a finite number of measurements (in our case, 29) might still miss the precession-driven changes. To test this possibility, we randomly selected 29 pairs of $\delta O_2/N_2$ and δD_{ice} data from the 800 kyr Dome C record in which Northern Hemisphere insolation is known to pace Antarctic temperature[18]. The correlation coefficient (*r*) of the 29 pairs

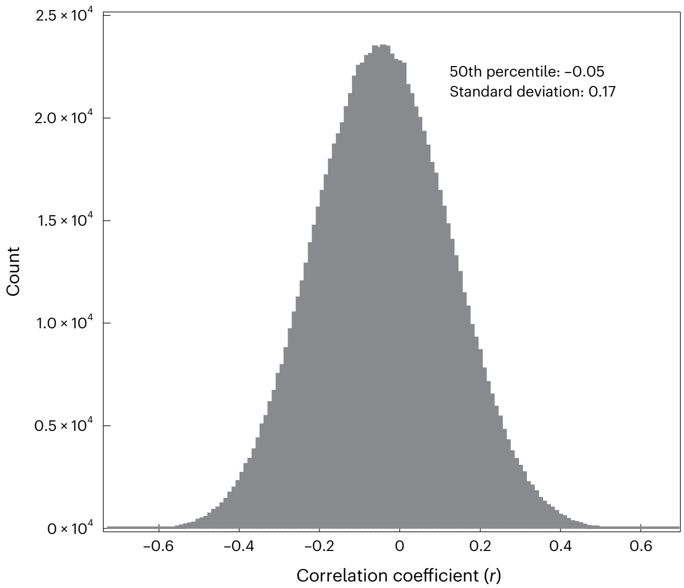

Fig. 4 | Testing the hypothesis of obliquity pacing of Antarctic temperature in the 40 kyr glacial cycles. The histogram shows the distribution of correlation coefficient r between 29 randomly selected Northern Hemisphere ISI (threshold insolation = 275 W m^{-2}, according to Huybers[6]) and Southern Hemisphere (77° S) 21 December insolation between 1.4 Ma and 2.1 Ma. 10^6 iterations were performed. Histogram bin width is 0.01.

of data points was subsequently calculated. The process was repeated 10^6 times, resulting in a distribution of the correlation coefficient (Fig. 3). The estimated r is 0.20 ± 0.17 (1σ), meaning that the statistically significant negative correlation between the 29 $\delta O_2/N_2$ and δD_{ice} data points obtained from the Allan Hills ice is not a sampling artefact.

Alternatively, the negative correlation could appear when the δD_{ice}, paced by Northern Hemisphere insolation, lags $\delta O_2/N_2$ (that is, local insolation) by half of a precession cycle (~11 kyr). However, in the Late Pleistocene, δD_{ice} in Antarctic ice lags Northern Hemisphere summer insolation only by ~2 kyr to 4 kyr in the precession band[16], less than a quarter of the full precession cycle length. In addition, it is inconceivable that $\delta O_2/N_2$ would lead insolation by nearly ~8 kyr; instead, insolation leads $\delta O_2/N_2$ by no more than 6 kyr (refs. [25,26]). Taken together, the observed $\delta O_2/N_2$-δD_{ice} relationship cannot be explained by the hypothesis that Northern Hemisphere insolation paced Antarctic temperature in the Early Pleistocene.

Next, we consider the competing hypothesis that Antarctic temperature responded only to obliquity pacing in the Early Pleistocene, such as by Northern Hemisphere ISI above 275 W m^{-2} at 65° N that drives 40 kyr glacial cycles[6]. We repeated the Monte Carlo simulation described above, this time randomly selecting 29 pairs of 65° N summer ISI and 77° S 21 December insolation intensity data between 1.4 Ma and 2.1 Ma (reflecting the lower 95% CI of the 1.5 Ma and the upper 95% CI of the 2.0 Ma ages, respectively). Each iteration yields a correlation coefficient r. The distribution of r values from 10^6 iterations are shown as a histogram (Fig. 4). The Monte Carlo simulation yields a correlation coefficient of −0.05 ± 0.17 (1σ), but a correlation coefficient greater than 0.367 is required to yield a statistically significant ($p < 0.05$; two-tailed) correlation given the sample size ($N = 29$). Therefore, the ISI and Southern Hemisphere insolation are not positively correlated. The observed δD_{ice}–$\delta O_2/N_2$ relationship is not compatible with the hypothesis that Northern Hemisphere ISI paced Antarctic temperature in the 40 kyr glacial cycles. Even if that were the case, it is unclear why precession signals, which can only explain approximately 20% of the variance in the 65° N summer ISI[7], became manifest in the ice core archives after the MPT.

Having considered and excluded two alternative explanations, we conclude that the observed negative correlation between the δD_{ice} and $\delta O_2/N_2$ in 1.5 Ma and 2.0 Ma samples is best explained by Antarctic temperature being paced by local Southern Hemisphere insolation in the Early Pleistocene. This result supports the hypothesis first put forward in Raymo et al.[8] that the absence of precession forcing in the 40 kyr cycles is due to out-of-phase growth and decay of bipolar ice sheets. Further support for this hypothesis include precession-related oscillations in grain-size data (an indirect proxy for climate) from Lake El'gygytgyn in northeast Russia[43] and marine records from the Gulf of Mexico suggesting that the Laurentide Ice Sheet was sensitive to precession forcing in the Early Pleistocene[44]. A recent record of North Atlantic ice rafting also provides strong evidence for the persistent influence of precession on ice losses, although this record can neither confirm nor reject that 'pre-MPT ice sheets varied strongly at precession frequencies'[45]. Here Antarctic ice cores paint a complementary picture in the south. After the MPT, Antarctic temperature became paced by Northern Hemisphere insolation[16–18], possibly due to the growth of the EAIS from being land based into marine terminating that made ice loss sensitive to sea level forcing paced by Northern Hemisphere insolation in the Late Pleistocene[8,46]. However, we acknowledge that our ice core records cannot identify the immediate or ultimate cause(s) of this Antarctic ice volume change.

Oxygen-to-nitrogen ratios in the trapped air in discontinuous blue ice records from the Allan Hills, East Antarctica, extending to the Early Pleistocene serve as a proxy for local 21 December insolation intensity (lower $\delta O_2/N_2$ corresponds to higher insolation). A negative correlation between ice core δD_{ice} values and $\delta O_2/N_2$ ratios before the MPT indicates that Antarctic temperature was positively correlated with local insolation in the 40 kyr glacial cycles. The sign of the $\delta O_2/N_2$–δD_{ice} relationship flipped across the MPT. This result is best explained by the hypothesis that in the Early Pleistocene, precession forcing is absent in the global $\delta^{18}O$ record of benthic foraminifera because climate change in the precession band was out of phase between the two hemispheres[8,9].

Online content

Any methods, additional references, Nature Portfolio reporting summaries, source data, extended data, supplementary information, acknowledgements, peer review information; details of author contributions and competing interests; and statements of data and code availability are available at https://doi.org/10.1038/s41561-022-01095-x.

References

1. Imbrie, J. et al. On the structure and origin of major glaciation cycles 1. linear responses to Milankovitch forcing. *Paleoceanography* **7**, 701–738 (1992).
2. Lisiecki, L. E. & Raymo, M. E. A Pliocene–Pleistocene stack of 57 globally distributed benthic $\delta^{18}O$ records. *Paleoceanography* **20**, PA1003 (2005).
3. Hays, J. D., Imbrie, J. & Shackleton, N. J. Variations in the Earth's orbit: pacemaker of the ice ages: for 500,000 years, major climatic changes have followed variations in obliquity and precession. *Science* **194**, 1121–1132 (1976).
4. Berends, C. J., Köhler, P., Lourens, L. J. & van de Wal, R. S. W. On the cause of the mid-Pleistocene transition. *Rev. Geophys.* **59**, e2020RG000727 (2021).
5. Raymo, M. E. & Huybers, P. Unlocking the mysteries of the ice ages. *Nature* **451**, 284–285 (2008).
6. Huybers, P. Early Pleistocene glacial cycles and the integrated summer insolation forcing. *Science* **313**, 508–511 (2006).
7. Huybers, P. & Tziperman, E. Integrated summer insolation forcing and 40,000-year glacial cycles: the perspective from an ice-sheet/energy-balance model. *Paleoceanography* **23**, PA1208 (2008).

8. Raymo, M. E., Lisiecki, L. E. & Nisancioglu, K. H. Plio–Pleistocene ice volume, Antarctic climate, and the global $\delta^{18}O$ record. *Science* **313**, 492–495 (2006).
9. Morée, A. L. et al. Cancellation of the precessional cycle in $\delta^{18}O$ records during the Early Pleistocene. *Geophys. Res. Lett.* **48**, e2020GL090035 (2021).
10. McKay, R. et al. Pleistocene variability of Antarctic Ice Sheet extent in the Ross Embayment. *Quat. Sci. Rev.* **34**, 93–112 (2012).
11. Scherer, R. P. et al. Antarctic records of precession-paced insolation-driven warming during early Pleistocene Marine Isotope Stage 31. *Geophys. Res. Lett.* **35**, L03505 (2008).
12. Patterson, M. O. et al. Orbital forcing of the East Antarctic Ice Sheet during the Pliocene and Early Pleistocene. *Nat. Geosci.* **7**, 841–847 (2014).
13. Reilly, B. T. et al. New magnetostratigraphic insights from iceberg alley on the rhythms of Antarctic climate during the Plio–Pleistocene. *Paleoceanogr. Paleoclimatol.* **36**, e2020PA003994 (2021).
14. Petit, J. R. et al. Climate and atmospheric history of the past 420,000 years from the Vostok ice core, Antarctica. *Nature* **399**, 429–436 (1999).
15. Jouzel, J. et al. Orbital and millennial Antarctic climate variability over the past 800,000 years. *Science* **317**, 793–796 (2007).
16. Kawamura, K. et al. Northern Hemisphere forcing of climatic cycles in Antarctica over the past 360,000 years. *Nature* **448**, 912–916 (2007).
17. Suwa, M. & Bender, M. L. Chronology of the Vostok ice core constrained by O_2/N_2 ratios of occluded air, and its implication for the Vostok climate records. *Quat. Sci. Rev.* **27**, 1093–1106 (2008).
18. Bazin, L. et al. Phase relationships between orbital forcing and the composition of air trapped in Antarctic ice cores. *Clim. Past* **12**, 729–748 (2016).
19. Huybers, P. & Denton, G. Antarctic temperature at orbital timescales controlled by local summer duration. *Nat. Geosci.* **1**, 787–792 (2008).
20. Yan, Y. et al. Two-million-year-old snapshots of atmospheric gases from Antarctic ice. *Nature* **574**, 663–666 (2019).
21. Spaulding, N. E. et al. Ice motion and mass balance at the Allan Hills Blue-Ice Area, Antarctica, with implications for paleoclimate reconstructions. *J. Glaciol.* **58**, 399–406 (2012).
22. Kehrl, L. et al. Evaluating the duration and continuity of potential climate records from the Allan Hills Blue Ice Area, East Antarctica. *Geophys. Res. Lett.* **45**, 4096–4104 (2018).
23. Bender, M. L., Barnett, B., Dreyfus, G., Jouzel, J. & Porcelli, D. The contemporary degassing rate of ^{40}Ar from the solid Earth. *Proc. Natl Acad. Sci. USA* **105**, 8232–8237 (2008).
24. Higgins, J. A. et al. Atmospheric composition 1 million years ago from blue ice in the Allan Hills, Antarctica. *Proc. Natl Acad. Sci. USA* **112**, 6887–6891 (2015).
25. Landais, A. et al. Towards orbital dating of the EPICA Dome C ice core using $\delta O_2/N_2$. *Clim. Past* **8**, 191–203 (2012).
26. Extier, T. et al. On the use of $\delta^{18}O_{atm}$ for ice core dating. *Quat. Sci. Rev.* **185**, 244–257 (2018).
27. Haeberli, M. et al. Snapshots of mean ocean temperature over the last 700,000 years using noble gases in the EPICA Dome C ice core. *Clim. Past* **17**, 843–867 (2021).
28. Oyabu, I. et al. Fractionation of O_2/N_2 and Ar/N_2 in the Antarctic ice sheet during bubble formation and bubble–clathrate hydrate transition from precise gas measurements of the Dome Fuji ice core. *Cryosphere* **15**, 5529–5555 (2021).
29. Bender, M. L. Orbital tuning chronology for the Vostok climate record supported by trapped gas composition. *Earth Planet. Sci. Lett.* **204**, 275–289 (2002).
30. Yan, Y. et al. Enhanced moisture delivery into Victoria Land, East Antarctica during the early last interglacial: implications for West Antarctic Ice Sheet stability. *Clim. Past* **17**, 1841–1855 (2021).
31. Yan, Y., Brook, E. J., Kurbatov, A. V., Severinghaus, J. P. & Higgins, J. A. Ice core evidence for atmospheric oxygen decline since the Mid-Pleistocene transition. *Sci. Adv.* **7**, eabj9341 (2021).
32. Craig, H., Horibe, Y. & Sowers, T. Gravitational separation of gases and isotopes in polar ice caps. *Science* **242**, 1675–1678 (1988).
33. Stolper, D. A., Bender, M. L., Dreyfus, G. B., Yan, Y. & Higgins, J. A. A Pleistocene ice core record of atmospheric O_2 concentrations. *Science* **353**, 1427–1430 (2016).
34. Keeling, R. F. & Graven, H. D. Insights from time series of atmospheric carbon dioxide and related tracers. *Annu. Rev. Environ. Resour.* **46**, 85–110 (2021).
35. Fujita, S., Okuyama, J., Hori, A. & Hondoh, T. Metamorphism of stratified firn at Dome Fuji, Antarctica: a mechanism for local insolation modulation of gas transport conditions during bubble close off. *J. Geophys. Res. Earth Surf.* **114**, F03023 (2009).
36. Dansgaard, W. Stable isotopes in precipitation. *Tellus* **16**, 436–468 (1964).
37. Kavanaugh, J. L. & Cuffey, K. M. Generalized view of source-region effects on δD and deuterium excess of ice-sheet precipitation. *Ann. Glaciol.* **35**, 111–117 (2002).
38. Holloway, M. D. et al. Antarctic last interglacial isotope peak in response to sea ice retreat not ice-sheet collapse. *Nat. Commun.* **7**, 12293 (2016).
39. Uemura, R. et al. Asynchrony between Antarctic temperature and CO_2 associated with obliquity over the past 720,000 years. *Nat. Commun.* **9**, 961 (2018).
40. Kobashi, T. et al. Post-bubble close-off fractionation of gases in polar firn and ice cores: effects of accumulation rate on permeation through overloading pressure. *Atmos. Chem. Phys.* **15**, 13895–13914 (2015).
41. Bereiter, B., Fischer, H., Schwander, J. & Stocker, T. F. Diffusive equilibration of N_2, O_2 and CO_2 mixing ratios in a 1.5-million-years-old ice core. *Cryosphere* **8**, 245–256 (2014).
42. Spaulding, N. E. et al. Climate archives from 90 to 250 ka in horizontal and vertical ice cores from the Allan Hills Blue Ice Area, Antarctica. *Quat. Res.* **80**, 562–574 (2013).
43. Francke, A. et al. Multivariate statistic and time series analyses of grain-size data in Quaternary sediments of Lake El'gygytgyn, NE Russia. *Clim. Past* **9**, 2459–2470 (2013).
44. Shakun, J. D., Raymo, M. E. & Lea, D. W. An Early Pleistocene Mg/Ca-$\delta^{18}O$ record from the Gulf of Mexico: evaluating ice sheet size and pacing in the 41-kyr world. *Paleoceanography* **31**, 1011–1027 (2016).
45. Barker, S. et al. Persistent influence of precession on northern ice sheet variability since the early Pleistocene. *Science* **376**, 961–967 (2022).
46. Elderfield, H. et al. Evolution of ocean temperature and ice volume through the mid-Pleistocene climate transition. *Science* **337**, 704–709 (2012).
47. Laskar, J. et al. A long-term numerical solution for the insolation quantities of the Earth. *Astron. Astrophys.* **428**, 261–285 (2004).

Methods

Glaciological setting of the Allan Hills Blue Ice Area

Allan Hills (76.73° S, 159.36° E) is situated ~100 km to the northwest of the McMurdo Dry Valleys and the Convoy Range in Victoria Land, East Antarctica, and ~80 km from the Ross Sea coastline. In the Allan Hills Blue Ice Area, main ice flow is from the southwest to the northeast, partially blocked and diverted by the Allan Hills. Local meteorological conditions and surface snow and ice properties are documented in detail by Dadic et al.[48]. The glaciological setting means that ancient ice once buried deep in the ice sheet is being transported towards the surface[49]. After overriding a series of subglacial mountains, the ice eventually drains into the Ross Sea embayment via the Mawson Glacier[50].

Allan Hills ice samples used in this study are from three adjacent boreholes: Site 27 (S27; 76.70° S, 159.31° E; drilled in 2010), ALHIC1502 (76.73286° S, 159.35507° E; drilled in 2015) and ALHIC1503 (76.73243° S, 159.3562° E; drilled in 2015). S27 is located on the main ice flow line and provides a continuous ice record between approximately 115 ka and 255 ka (refs. [30,42]). It has been under the custody of Climate Change Institute, University of Maine and stored in a freezer in Bangor, Maine, since retrieval. Stratigraphically discontinuous samples dating beyond 1.0 Ma came from ALHIC1502 and ALHIC1503, two sites disconnected from the main ice flow line on a steep (approximately 45°) bedrock leading to a local bedrock high[20,24]. These samples have been stored at the National Science Foundation Ice Core Facility since recovery. At Allan Hills, low basal temperature further inhibits glacial flow and promotes the preservation of exceptionally old (>2 Ma) ice samples. The measured oldest ice from this region is 2.7 Ma ± 0.3 Ma (1σ). The gas composition in this oldest ice has unfortunately been altered by in situ production of CO_2 (ref. [20]) and the $\delta O_2/N_2$ is not reliable as well[31].

Timescale development for stratigraphically discontinuous ice

Ice samples from ALHIC1502 and ALHIC1503 were dated by measuring the gravitationally corrected $^{40}Ar/^{38}Ar$ ratios ($^{40}Ar_{atm} = \delta^{40}Ar/^{38}Ar - \delta^{38}Ar/^{36}Ar$) in the trapped gases. Details of the analytical procedures have been described in Higgins et al.[24] and Yan et al.[20]. In brief, this method takes advantage of the fact that ^{40}Ar, a product of the radioactive decay of solid Earth ^{40}K, slowly leaks into and accumulates in the atmosphere[23]. The minor isotopes of argon (^{38}Ar and ^{36}Ar), by contrast, are primordial, non-radiogenic and stable. The $^{40}Ar/^{38}Ar$ ratio, after correcting for gravitational fractionation using $^{38}Ar/^{36}Ar$ ratios, increases with time going forward at an empirically determined rate of 0.066 ± 0.006 ‰ Myr^{-1} over the past 800,000 years (ref. [23]). This means that the air trapped in the ice can be dated without the prerequisite for stratigraphic continuity or assumptions involved in orbital dating. The latter is crucial to the evaluation of orbital forcing's role (or lack thereof) in Antarctic climate variations.

Stable water isotope data description

The Allan Hills stable water isotope data have been reported in Yan et al.[20] for ALHIC1502 and ALHIC1503 and in Spaulding et al.[42] for S27 ice. We provide only a brief description of the analytical procedures here. A typical ice sample for stable water isotope analyses measures 10 cm to 15 cm in length. Each individual ice sample was melted in a sealed bag, and the meltwater was transferred into a plastic vial. $\delta^{18}O_{ice}$ and δD_{ice} analyses were performed simultaneously on a Picarro Model L2130-i Ultra High-Precision Isotopic Water Analyser housed in Climate Change Institute, University of Maine. The internal precision (2σ) is ± 0.05‰ for $\delta^{18}O_{ice}$ and ± 0.10‰ for δD_{ice}. Final values are expressed as per mil (‰) with respect to the internationally recognized water isotope standard V-SMOW. Dome Fuji, Vostok and Dome C δD_{ice} data are reported by Uemura et al.[39], Petit et al.[14] and Landais et al.[51], respectively.

$\delta O_2/N_2$ and $\delta Ar/N_2$ data description

Complete $\delta O_2/N_2$ and $\delta Ar/N_2$ data from ALHIC1502 and ALHIC1503 cores have recently been published in Yan et al.[31]. The cited work also describes the analytical procedures (modified from Dreyfus et al.[52]) of elemental and isotopic ratio measurements, the age assignment for each individual analysis (which deals with the fact that depths of samples measured for $O_2/N_2/Ar$ were different from depths of the $^{40}Ar_{atm}$ samples that constrained the chronology) and criteria for rejecting specific portions of the data. The pooled standard deviation (1σ) of the Allan Hills $\delta O_2/N_2$ and $\delta Ar/N_2$ measured in ALHIC1502 and ALHIC1503 cores is ± 3.37‰ and ± 2.08‰, respectively. Four age groups are identified for the Allan Hills $\delta O_2/N_2$ data: 400 ka, 810 ka, 1.5 Ma and 2.0 Ma. Each of these ages refers to a cluster of $^{40}Ar_{atm}$ dates. The 400 ka and 810 ka groups represent the post-MPT and MPT glacial cycles, respectively. Early Pleistocene glacial cycles are represented by the combined 1.5 Ma and 2.0 Ma group. In this study, we followed most of the data rejection criteria adopted by Yan et al.[31], apart from the four 2.0 Ma $\delta O_2/N_2$ samples rejected in that study. These four data points were not included in Yan et al.[31] because the cited work concerns the secular change of atmospheric O_2 concentration and 1.5 Ma and 2.0 Ma samples potentially represent two distinct age groups. Four data points are insufficient to fully characterize the 2.0 Ma age bin. However, both 1.5 Ma and 2.0 Ma samples are part of the 40 kyr glacial cycles, and no long-term δD_{ice} change is observed between 1.5 Ma and 2.0 Ma ice (Fig. 2 in ref. [20]). The four 2.0 Ma samples are therefore retained in this study.

$\delta O_2/N_2$ data from the continuous Allan Hills S27 core exist in two batches: those reported by Yan et al.[30] and those included in Spaulding et al.[42]. The pooled standard deviation (1σ) of the S27 $\delta O_2/N_2$ reported in Yan et al.[30] and Spaulding et al.[42] is ± 3.81‰ and ± 4.23‰, respectively. Samples below 140 m were further excluded from this study because ice below this depth is characterized by extensive fractures, resulting in substantial post-coring gas losses that completely overwhelm the primary insolation signals[30]. Above 140 m, there are 13 $\delta O_2/N_2$ data from Spaulding et al.[42] and 26 $\delta O_2/N_2$ data from Yan et al.[30]. Apart from the smaller number, data reported by Spaulding et al.[42] were measured using the analytical protocol used by Higgins et al.[24]. In that protocol, the glass vessel holding ice core samples was pumped for an indefinite amount of time until the residual air pressure reached 0.7 mTorr. This approach introduces a varying degree of gas losses to individual ice samples, even though samples measured by Spaulding et al.[42] experience fewer degrees of gas loss fractionation during storage compared with those more recently measured by Yan et al.[30]. This methodological feature also accounts for why the ALHIC1503 data above 126 m reported in Higgins et al.[24] were rejected in Yan et al.[31] (and by extension here as well). On the other hand, the analytical method for the S27 $\delta O_2/N_2$ samples reported by Yan et al.[30] is the same as the protocol for the ALHIC1502 and ALHIC1503 ice used in this study[31]. In each gas extraction process, ice was subject to 3 min pumping by a turbomolecular pump. Though still expected to be present, gas loss fractionation should be more or less uniform across samples. This difference perhaps explains why the S27 $\delta O_2/N_2$ data measured in Yan et al.[30] has smaller pooled standard deviation (± 3.81‰; 1σ) than those measured earlier in Spaulding et al. (± 4.23‰; 1σ) (ref. [42]). As a result, we opted to use the more recent dataset reported by Yan et al.[30]. Here we also report the accompanying S27 $\delta Ar/N_2$ data. In this S27 dataset, two samples above approximately 21 m were rejected because contamination by modern air has been observed in depth up to 7 m to 10 m (ref. [42]). The remaining depth interval (21 m to 140 m) corresponds to 119 ka to 144 ka, covering a full precession cycle and 60% of an obliquity cycle, which explains why the S27 $\delta O_2/N_2$ data do not span the full range of insolation values in Fig. 1d. The total number of S27 gas samples used in this study is 24, each with at least one replicate analysis (Extended Data Fig. 7). These 24 samples, and ALHIC1502 and ALHIC1503 samples reported by Yan et al.[31] and used in this study, have no fractures in them.

Other deep ice core $\delta O_2/N_2$ data have been previously published, and we provide only a synthesis here (with some additional corrections to apply; next section and Extended Data Table 1). In deep ice cores, the transition from bubbles to clathrates (bubble–clathrate transition

 https://doi.org/10.1038/s41561-022-01095-x

zone; BCTZ) leads to large fractionation of $\delta O_2/N_2$ and $\delta Ar/N_2$ in the two phases due to solubility differences[28,53–55]. We therefore excluded data from the BCTZ in all deep ice cores.

Dome Fuji $\delta O_2/N_2$ data are reported in two studies: Kawamura et al.[16] and Oyabu et al.[28], the latter of which further includes the $\delta Ar/N_2$ data (measured simultaneously with $\delta O_2/N_2$) used in this study. Samples above 450 m in Dome Fuji core trap air only in bubbles, and the trapped gases exist in the form of clathrate only and below 1,200 m (ref. [54]).

Dome C $\delta O_2/N_2$ data are based on a series of studies listed in chronological order: Landais et al.[25], Bazin et al.[18], Extier et al.[26] and Haeberli et al.[27]. $\delta Ar/N_2$ data are from Haeberli et al.[27] only. Although Stolper et al.[33] reports $\delta Ar/N_2$ data from the Dome C ice (previously unpublished data measured as part of the Ph.D thesis of Dreyfus[56]), they do not have corresponding $\delta O_2/N_2$ data measured on the same ice and were excluded from this study. In the Dome C core, gases exist as bubbles in samples younger than 50 ka and as clathrate in samples older than 100 ka. There is no reported $\delta O_2/N_2$ data from the BCTZ in the Dome C ice core.

Vostok $\delta O_2/N_2$ data are from Bender[29] with companion $\delta Ar/N_2$ data first reported in Stolper et al.[33]. Above ~500 m, the trapped gases exist as bubbles and completely transform into clathrate below ~1,200 m in Vostok[53]. Intriguingly, Bender[29] observes large residual scatter in samples up to ~1,700 m, despite the fact that bubbles have already disappeared. The origin of this residual scatter is perhaps due to the clathrate layering within the ice and differential diffusion of O_2 and N_2 in the growing clathrate[57,58], which eventually disappears at depth by diffusive homogenization. In any case, we include only Vostok ice samples deeper than 1,760 m (approximately 125 ka in age) in this study. Including shallower (noisier) clathrate data increases the scatter in $\delta O_2/N_2$ but does not invalidate the use of $\delta O_2/N_2$ as a proxy for local insolation intensity.

Correction for secular O_2 changes

Because we are interested only in O_2/N_2 and Ar/N_2 variations associated with bubble close-off fractionation, the long-term decline in atmospheric O_2 over the past 0.8 Myr (refs. [31,33]), and ongoing changes associated with the combustion of fossil fuels[34], needs to be corrected for as follows.

A long-term, natural decline in the $\delta O_2/N_2$ ratio has been found in Dome Fuji, Vostok and Dome C ice cores used in this study[25,26,33]. The decline, with an observed rate of 8.4 ± 0.2‰ Myr^{-1} (1σ), is interpreted to reflect a decrease in the atmospheric O_2 burden[33] beginning at ~800 ka (ref. [31]). We correct for higher past values by subtracting $t \times 8.4 / 1{,}000$ from the measured values:

$$\delta O_2/N_{2,\text{long-term}} = \delta O_2/N_2 - t \times 8.4/1,000. \qquad (1)$$

t is age of the ice in kyr. For samples older than 800 ka in ALHIC1502 and ALHIC1503, the correction is simply 800 × 8.4/1,000 (or subtracting 6.7‰ from the measured $\delta O_2/N_2$). Admittedly we do not know for sure if the O_2 concentration remained stable between 1.5 Ma and 2.0 Ma, but paired $\delta O_2/N_2$–$\delta Ar/N_2$ analyses suggest that the 2.0 Ma data do not fall outside the 95% prediction interval defined by the 1.5 Ma $\delta O_2/N_2$–$\delta Ar/N_2$ data pairs[31]. Nonetheless, if we assume that there was a decline with the same rate in the Late Pleistocene, the 2.0 Ma data would need to be lowered by 4.2‰. This would actually make the observed negative correlation even stronger. For young (<800 ka) samples in ALHIC1502, we used the weighted-average $^{40}Ar_{atm}$ age (400 ka) to account for the secular change in $\delta O_2/N_2$. We caution that in the 400 ka bin of the ALHIC1502 data, the age of the individual samples is not necessarily the same. That means the uniform correction will not accurately account for the long-term changes in individual $\delta O_2/N_2$ data within that age bin. However, given the age uncertainties of approximately ± 70 kyr (± 95% CI), the maximum impact of this secular change in the 400 ka age bin is about 1.2‰ or about 6% of the range of observed $\delta O_2/N_2$ (Fig. 2).

In addition to the natural change in PO_2 over the past 800 kyr, there has been a more rapid decline in PO_2 due to anthropogenic use of fossil fuel since the Industrial Revolution. On the basis of observations since 1990, the rate of anthropogenic PO_2 change is −0.019‰ per year (ref. [34]). Note that this process does not affect the composition of the trapped air inside the ice. However, this change will affect the reported $\delta O_2/N_2$ values because modern atmosphere is ultimately used as the standard against which the measured gas ratios are normalized. For instance, if we measure the exact same sample stored at −50 °C (thus no gas losses; Supplementary Information) ten years apart, the reported $\delta O_2/N_2$ value, after normalization to coeval atmosphere, measured ten years earlier will be 0.19‰ lower. For Allan Hills (including S27) and Vostok samples, this anthropogenic PO_2 change is not an issue because they are normalized to clean dry air collected around year 1990 in a high-pressure cylinder and are thus internally consistent. However, Dome Fuji and Dome C $\delta O_2/N_2$ data are obtained from samples measured from several years apart, so the varying composition of O_2 standard (atmosphere) is a potential problem. Below, we attempt to correct for this effect to the best of our knowledge.

Dome Fuji $\delta O_2/N_2$ data reported by Oyabu et al.[28] are measured in accordance with procedures described in Oyabu et al.[59] in which the modern air for $\delta O_2/N_2$ is defined as 'the annual average $\delta O_2/N_2$ in 2017 observed over Minamitorishima island'. Earlier Dome Fuji $\delta O_2/N_2$ data included in Kawamura et al.[16] were calibrated against Antarctic surface air collected in 1999 at site H72 and Dome Fuji[60].

Dome C ice core $\delta O_2/N_2$ data have a more complicated measurement history. The data published by Landais et al.[25], Bazin et al.[18] and Extier et al.[26] were normalized against air that was collected in 2005–2008, 2012–2013 and 2016, respectively. However, we could not differentiate the data measured in Landais et al.[25] and Bazin et al.[18], so we use year 2009 as their collection year (the average of 2005 and 2013). The ± 4 years will introduce an error up to ± 0.08‰ in $\delta O_2/N_2$, less than 2% of the observed range of Dome C $\delta O_2/N_2$ data (approximately 11‰). The most recent Dome C dataset reported by Haeberli et al.[27] uses 'a modern atmosphere standard collected outside the lab in Bern, Switzerland'. The air standard was collected from February 2016 to December 2017, as documented in Marcel Haeberli's Ph.D thesis[61]. We use the collection year of 2016.

Extended Data Table 1 summarizes the time of collection of air standards used by different studies. The final reported data, $\delta O_2/N_{2,\text{fossil fuel corr}}$, as shown in Figs. 1 and 2, are normalized to air standard in year 1990, the year when the observation of PO_2 began[34]:

$$\delta O_2/N_{2,\text{fossil fuel corr}} = \delta O_2/N_{2,\text{long-term}} - (\text{year} - 1990) \times 19/10^6. \qquad (2)$$

'year' is the collection year for the reference of a specific dataset. By definition, the correction is zero for references collected in 1990. All the Dome Fuji and Dome C $\delta O_2/N_2$ data have been corrected for the drift in air standard composition due to anthropogenic PO_2 change on the basis of the year of collection of their air standards.

Impact of analytical uncertainties in $\delta O_2/N_2$ and $\delta Ar/N_2$ on correlation robustness

In this study, we used an ordinary least square linear regression to evaluate if δD_{ice} (dependent variable) is correlated with insolation proxies–$\delta O_2/N_2$ or $\delta Ar/N_2$ (independent variable; Fig. 2 and Extended Data Fig. 5). The ordinary least square regression attributes the scatter in the dependent variable to random noise and assumes no errors in the independent variable. This assumption is problematic in the case of δD_{ice}–$\delta O_2/N_2$ and δD_{ice}–$\delta Ar/N_2$ correlations, because $\delta O_2/N_2$ and $\delta Ar/N_2$ data have considerable analytical errors compared with their range. By contrast, the analytical uncertainties associated with δD_{ice} measurements are much smaller (internal precision = 0.05‰ (1σ)).

To quantitatively evaluate the robustness of the observed negative correlation between δD_{ice} and $\delta O_2/N_2$ (or $\delta Ar/N_2$) from 1.5 Ma and 2.0 Ma ice, we performed a Monte Carlo simulation that explicitly considers the uncertainties associated with the $\delta O_2/N_2$ and $\delta Ar/N_2$ data. In each iteration, a synthetic $\delta O_2/N_2$ (or $\delta Ar/N_2$) record is generated based on the actual measured value and the analytical uncertainties (1σ; 2.38‰ for $\delta O_2/N_2$ and 1.47‰ for $\delta Ar/N_2$), assuming a Gaussian distribution. Note the analytical uncertainties used here are smaller than the pooled standard deviations of those measurements because two pairs of replicates were measured for each depth. The pooled standard deviations are thus divided by the square root of 2. A total number of 10^6 iterations were performed, resulting in 10^6 correlation coefficients between δD_{ice} and $\delta O_2/N_2$ (or $\delta Ar/N_2$). On the basis of the distribution of the calculated r values, we seek to answer the following question: what is the probability that the observed correlation becomes statistically insignificant when errors are considered?

For the negative correlation to be significant at 0.05 level (one-tailed) given the sample size (N = 29 in 1.5 Ma and 2.0 Ma samples), a r value more negative than −0.311 is required. We used the one-tailed p value here because the hypothesis being evaluated is that the correlation is negative rather than there is a non-insignificant correlation, in which case p values need to be two-tailed. We then compared this critical r value (−0.311) to the 95th percentile in those 10^6 simulated r values derived between δD_{ice} and $\delta O_2/N_2$ (−0.331; Fig. 3) and between δD_{ice} and $\delta Ar/N_2$ (−0.272; Extended Data Fig. 5). If the 95th percentile r value is smaller than the critical r, −0.311, it means that there is less than 5% chance that the negative correlation will cease to exist. In this scenario, the correlation is considered robust, which is the case for the $\delta O_2/N_2$–δD_{ice} relationship. The robustness of correlation does not hold for δD_{ice} and $\delta Ar/N_2$, however, possibly because in terms of insolation, the signal-to-noise ratio of $\delta Ar/N_2$ is smaller than the same ratio registered in $\delta O_2/N_2$, visually evidenced by the length of the error bars relative to the x axis in Fig. 2 and Extended Data Fig. 5.

Data availability

All data supporting the conclusion of this paper are publicly available without restriction. Dome Fuji, Dome C and Vostok data are from data depositories associated with their respective publications. Allan Hills gas ratio and stable water isotope data are available at the US Antarctic Program Data Center: https://doi.org/10.15784/601483 (ALHIC1502 and ALHIC1503 $O_2/N_2/Ar$ elemental and isotopic ratios), https://doi.org/10.15784/601129 (ALHIC1502 stable water isotopes), https://doi.org/10.15784/601128 (ALHIC1503 stable water isotopes), https://doi.org/10.15784/601512 (S27 $\delta O_2/N_2$ and $\delta Ar/N_2$ ratios) and https://doi.org/10.7265/N5NP22DF (S27 stable water isotope records). We compiled those $\delta O_2/N_2$ and $\delta Ar/N_2$ data here as Supplementary Data 1 and 2, respectively. Source data for Figs. 3 and 4, and Extended Data Figure 5 are provided with this paper.

Code availability

MATLAB codes for the Monte Carlo simulation performed in this study are available at GitHub: https://github.com/yuzheny/MonteCarlo_correlation.

References

48. Dadic, R., Schneebeli, M., Bertler, N. A. N., Schwikowski, M. & Matzl, M. Extreme snow metamorphism in the Allan Hills, Antarctica, as an analogue for glacial conditions with implications for stable isotope composition. *J. Glaciol.* **61**, 1171–1182 (2015).
49. Whillans, I. M. & Cassidy, W. A. Catch a falling star: meteorites and old ice. *Science* **222**, 55–57 (1983).
50. Delisle, G. & Sievers, J. Sub-ice topography and meteorite finds near the Allan Hills and the near Western Ice Field, Victoria Land, Antarctica. *J. Geophys. Res. Planets* **96**, 15577–15587 (1991).
51. Landais, A. et al. Interglacial Antarctic–Southern Ocean climate decoupling due to moisture source area shifts. *Nat. Geosci.* **14**, 918–923 (2021).
52. Dreyfus, G. B. et al. Anomalous flow below 2,700 m in the EPICA Dome C ice core detected using $\delta^{18}O$ of atmospheric oxygen measurements. *Clim. Past* **3**, 341–353 (2007).
53. Ikeda, T. et al. Extreme fractionation of gases caused by formation of clathrate hydrates in Vostok Antarctic ice. *Geophys. Res. Lett.* **26**, 91–94 (1999).
54. Ikeda-Fukazawa, T., Hondoh, T., Fukumura, T., Fukazawa, H. & Mae, S. Variation in N_2/O_2 ratio of occluded air in Dome Fuji Antarctic ice. *J. Geophys. Res. Atmospheres* **106**, 17799–17810 (2001).
55. Huber, C. & Leuenberger, M. Measurements of isotope and elemental ratios of air from polar ice with a new on-line extraction method. *Geochem. Geophys. Geosyst.* **5**, Q10002 (2004).
56. Dreyfus, G. B. *Dating an 800,000 Year Antarctic Ice Core Record Using the Isotopic Composition of Trapped Air*. Ph.D thesis, Princeton Univ. (2008).
57. Lüthi, D. et al. CO_2 and O_2/N_2 variations in and just below the bubble–clathrate transformation zone of Antarctic ice cores. *Earth Planet. Sci. Lett.* **297**, 226–233 (2010).
58. Shackleton, S. et al. Is the noble gas-based rate of ocean warming during the Younger Dryas overestimated? *Geophys. Res. Lett.* **46**, 5928–5936 (2019).
59. Oyabu, I. et al. New technique for high-precision, simultaneous measurements of CH_4, N_2O and CO_2 concentrations; isotopic and elemental ratios of N_2, O_2 and Ar; and total air content in ice cores by wet extraction. *Atmos. Meas. Tech.* **13**, 6703–6731 (2020).
60. Kawamura, K. *Variations of Atmospheric Components Over the Past 340,000 Years From Dome Fuji Deep Ice Core, Antarctica*. Ph.D thesis, Tohoku Univ. (2001).
61. Häberli, M. *Noble Gas Ratios in Polar Ice Cores: A New Proxy to Infer the Mean Ocean Temperature Over the Last 700 ka*. Ph.D thesis, Universität Bern. (2019).

Acknowledgements

Funding for this work was provided by US National Science Foundation with the following grant numbers: ANT-1443263 (J.A.H.) and ANT-1443306 (A.V.K and P.A.M.). We thank the US Ice Drilling Design and Operations (IDDO), M. Waszkiewicz, P. Kemeny, S. Mackay and K. Borek Air for assistance with the field work. We also thank R. Nunn and G. Hargreaves at the National Science Foundation Ice Core Facility for help with ice core sample processing and archiving. We thank M. Bender for the constructive comments and discussions.

Author contributions

Conceptualization: Y.Y. Methodology: J.A.H. and Y.Y. for gas ratios and A.V.K. and P.A.M. for stable water isotopes. Investigation: Y.Y. Visualization: Y.Y. Supervision: J.A.H., A.V.K. and P.A.M. Writing, original draft: Y.Y. Writing, review and editing: S.S., A.V.K., P.A.M. and J.A.H.

Competing interests

The authors declare no competing interests.

Additional information

Extended data is available for this paper at https://doi.org/10.1038/s41561-022-01095-x.

Supplementary information The online version contains supplementary material available at https://doi.org/10.1038/s41561-022-01095-x.

https://doi.org/10.1038/s41561-022-01095-x

Correspondence and requests for materials should be addressed to Yuzhen Yan.

Peer review information *Nature Geoscience* and the authors thank Ryu Uemura, Frederic Parrenin and the other, anonymous, reviewer(s) for their contribution to the peer review of this work. Primary Handling Editor(s): James Super, in collaboration with the *Nature Geoscience* team.

https://doi.org/10.1038/s41561-022-01095-x

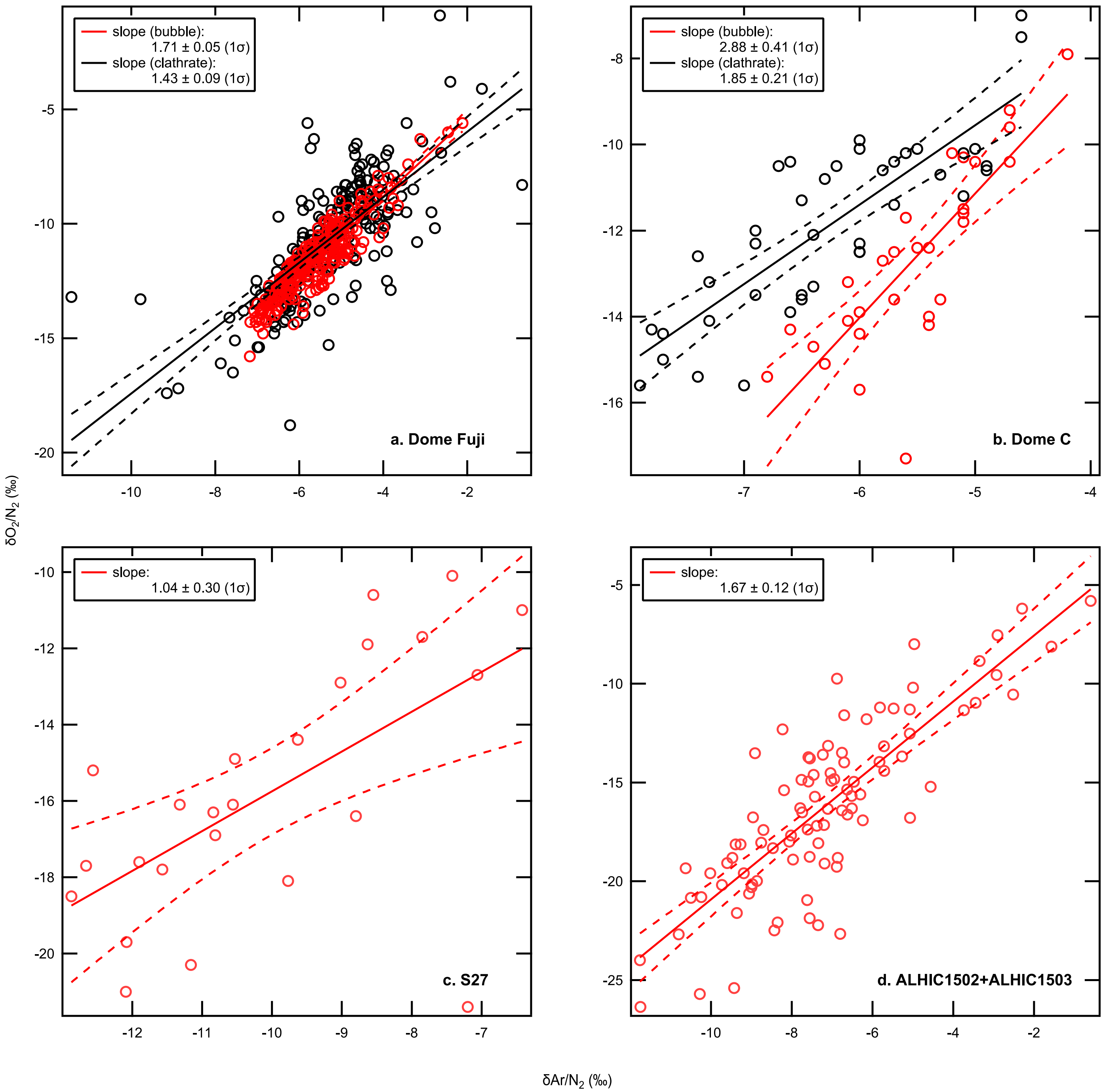

Extended Data Fig. 1 | Covariation between $\delta O_2/N_2$ and $\delta Ar/N_2$. a, Dome Fuji (clathrate $N = 219$, $r^2 = 0.52$; bubble $N = 238$, $r^2 = 0.82$); **b**, Dome C (clathrate $N = 40$, $r^2 = 0.68$; bubble $N = 29$, $r^2 = 0.66$); **c**, S27 ($N = 24$; $r^2 = 0.38$; and **d**, discontinuous Allan Hills ice ($N = 92$; $r^2 = 0.68$). Correlation in all samples regardless of gas preservation status are significant at $p = 0.05$ level (two-tailed). Part of this covariation is modulated by insolation. Clathrate- and bubble-based gas data are shown in black and red circles, respectively. Dashed lines represent 95% confidence interval of the slope. All of the Allan Hills samples only contain bubbles.

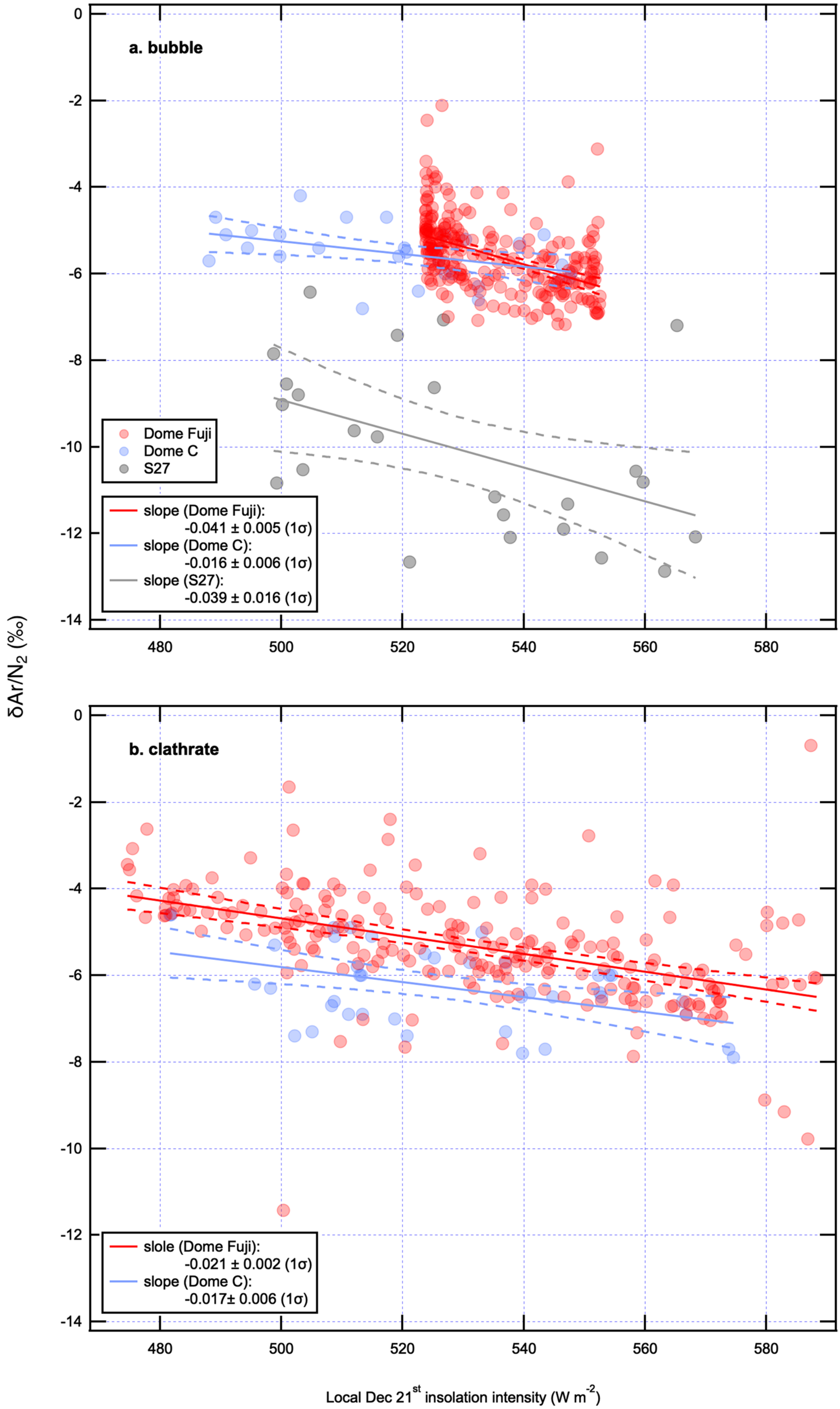

Extended Data Fig. 2 | See next page for caption.

Extended Data Fig. 2 | Insolation imprint in δAr/N_2 ratios of the air trapped in ice containing (a) bubbles and (b) clathrates only. The concept here is similar to Fig. 1 in the main text, with Dome Fuji (red)[28], Dome C (blue)[27], and Allan Hills S27 (gray)[30] datasets. Clathrate-based δAr/N_2 is negatively correlated with local Dec 21st insolation intensity in both Dome Fuji (sample $N = 219$, $r^2 = 0.24$, two-tailed $p < 0.01$) and Dome C ice ($N = 40$, $r^2 = 0.21$, $p < 0.01$). There is also a significant (two-tailed $p < 0.05$) correlation between bubble-based δAr/N_2 and insolation in Dome Fuji ($N = 238$, $r^2 = 0.24$), Dome C ($N = 29$, $r^2 = 0.20$), and S27 ($N = 24$, $r^2 = 0.23$) ice. Dashed lines represent 95% confidence interval of the slope. Note that the number of available δAr/N_2 data points is smaller than the number of δO_2/N_2 data, because not all δO_2/N_2-reporting studies include δAr/N_2.

 https://doi.org/10.1038/s41561-022-01095-x

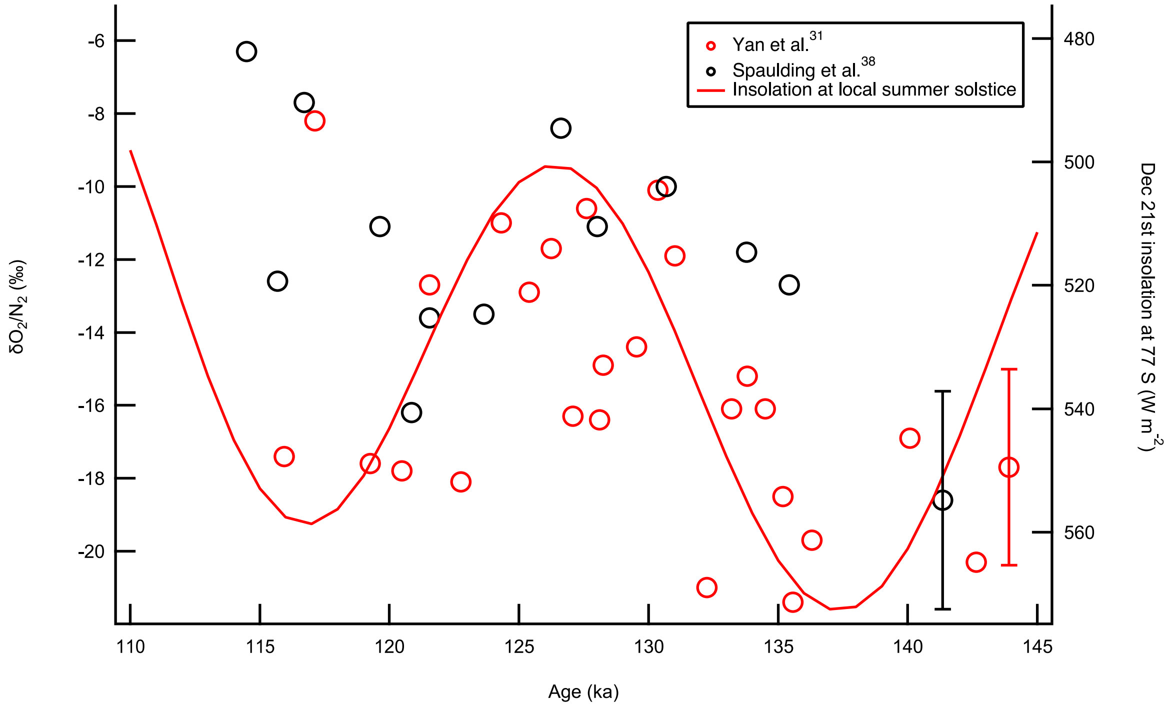

Extended Data Fig. 3 | S27 $\delta O_2/N_2$ data measured from ice above 140 m reported by Spaulding et al.[42] (black circles) and Yan et al.[30] (red circles) superimposed on the insolation at local (77 S) summer solstice. Error bars represent the pooled standard error of the $\delta O_2/N_2$ measurements reported by Spaulding et al.[42] (black; ± 2.99 ‰; unique sample number N = 38) and Yan et al.[30] (red; ± 2.69 ‰; unique sample number N = 45). Each unique samples have two replicates with the mean value reported. Note that the y-axis for insolation is reversed. The two shallowest $\delta O_2/N_2$ in Yan et al.[30] (marked by arrows) are not included in this study in view of suspected intrusion of modern air.

https://doi.org/10.1038/s41561-022-01095-x

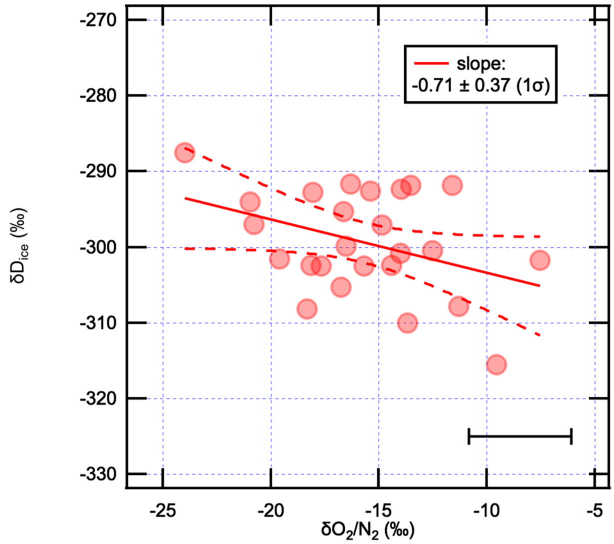

Extended Data Fig. 4 | Correlation between the isotopic composition of ice (δD_{ice}) and $\delta O_2/N_2$ of the trapped air in the Allan Hills blue ice dating back to 1.5 Ma. Error bars represent the pooled standard error of the $\delta O_2/N_2$ measurements (± 2.38 ‰). Dashed lines represent 95% confidence interval of the slope [−0.71 ± 0.37 (1σ)] of the linear regression. The correlation is not statistically significant at 95% significance level ($N = 25$; $r^2 = 0.15$; two-tailed $p = 0.06$).

https://doi.org/10.1038/s41561-022-01095-x

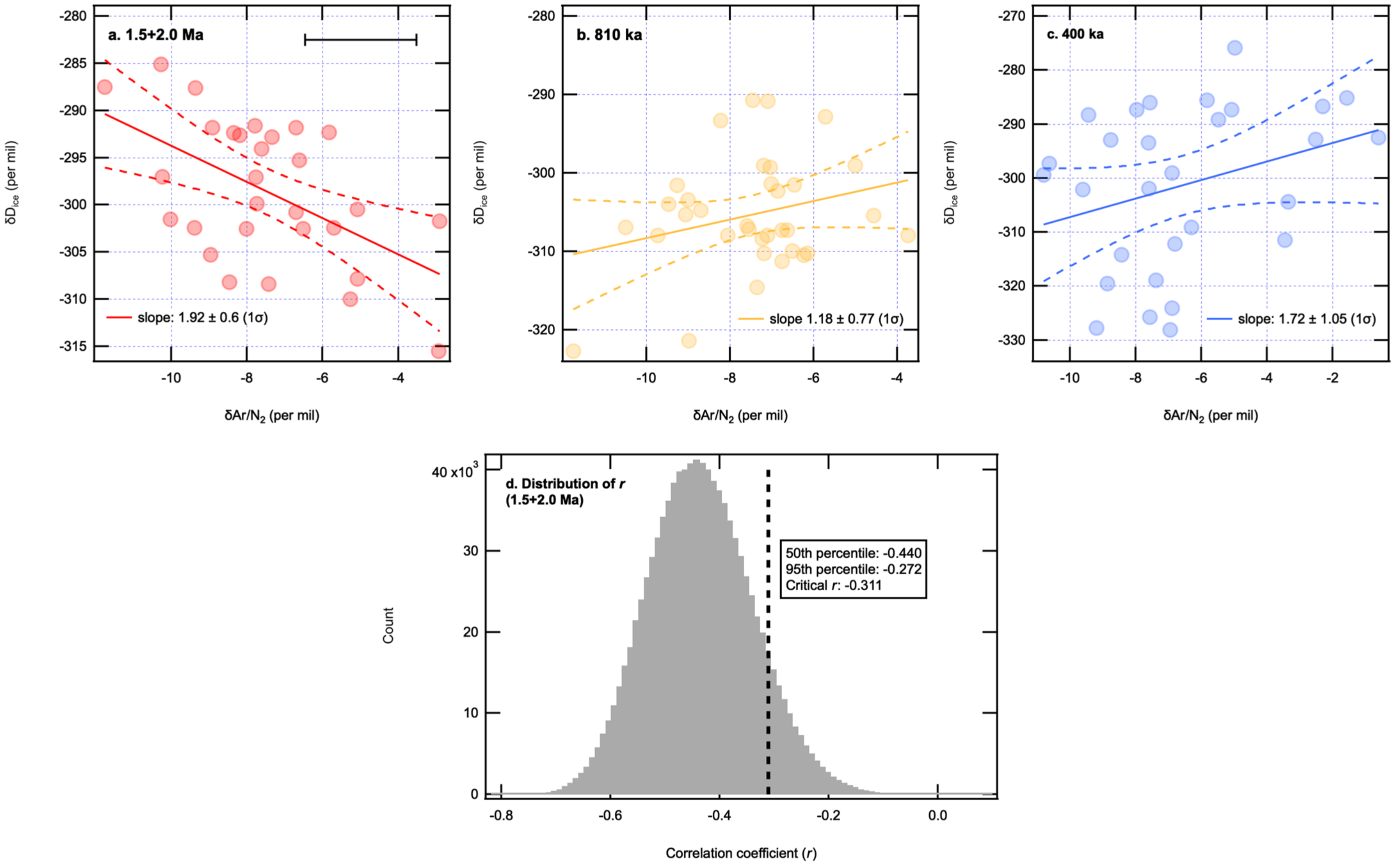

Extended Data Fig. 5 | Relationship of δD_{ice} and $\delta Ar/N_2$ of the trapped air in the Allan Hills ice and the robustness given analytical uncertainties. Panels (**a**-**c**) are conceptually very similar to Fig. 2 in the main text, but here $\delta Ar/N_2$ provides additional evidence to the observed negative correlation between δD_{ice} and $\delta O_2/N_2$ in samples dating back to 1.5 and 2.0 Ma. Error bars represent the pooled standard error of the $\delta Ar/N_2$ measurements (±1.47 ‰). Dashed lines represent 95% confidence interval. $\delta Ar/N_2$ is only significantly (two-tailed $p < 0.05$) correlated in the 1.5 and 2.0 Ma samples (sample $N = 29$, $r^2 = 0.28$), and not significantly correlated in the 810 ka ($N = 34$, $r^2 = 0.07$) or the 400 ka samples ($N = 29$, $r^2 = 0.10$). However, the 95th percentile of r value between the 29 $\delta Ar/N_2$ and δD_{ice} data pairs dating back to 1.5 and 2.0 Ma is −0.272 in a 10^6-iteration Monte Carlo simulation (panel **d**). Given the sample size ($N = 29$), the critical r value at 0.05 significance level (one-tailed) is −0.311 (dashed vertical line), meaning that there is a greater than 5% chance that the analytical uncertainties in $\delta Ar/N_2$ lead to insignificant correlation. The negative $\delta Ar/N_2$-δD_{ice} relationship is thus not considered robust. Histogram bin size is 0.01.

https://doi.org/10.1038/s41561-022-01095-x

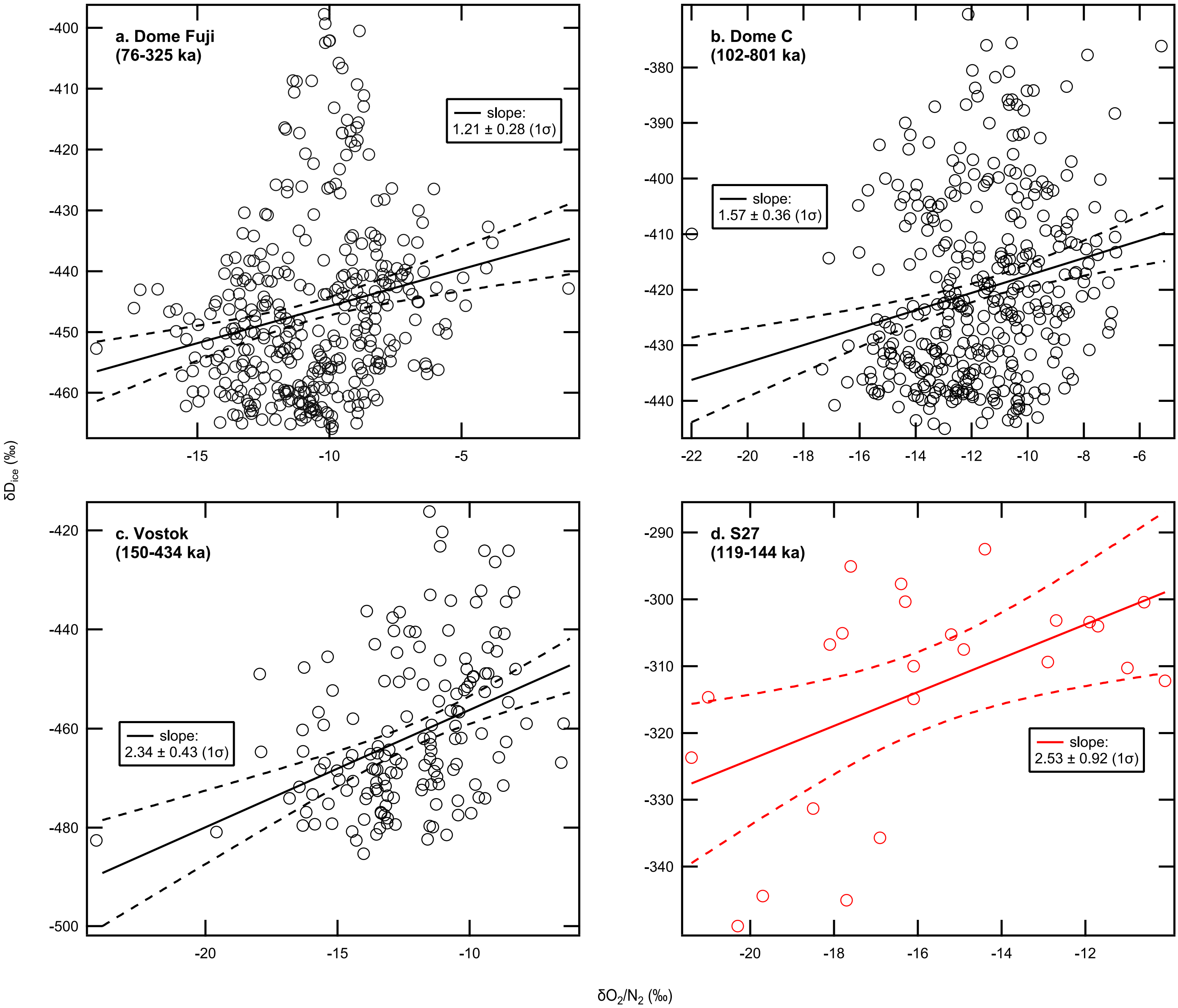

Extended Data Fig. 6 | Relationship between $\delta O_2/N_2$ and δD_{ice} measured from the same depth in (a) Dome Fuji[16,28,39], (b) Dome C[18,25–27,51], (c) Vostok[14,29], and (d) Allan Hills S27 ice. Only clathrate-based data from Dome Fuji, Dome C, and Vostok are used in this comparison, shown as black circles. A statistically significant (two-tailed $p < 0.01$) positive correlation exists in Dome Fuji ($N = 366$, $r^2 = 0.04$), Dome C ($N = 365$, $r^2 = 0.05$), and Vostok ($N = 151$, $r^2 = 0.16$) data. Red circles in S27 indicate that gas ratio data were measured on ice samples containing bubbles because the Allan Hills S27 ice has no clathrate. The correlation is still positive and significant ($N = 24$, $r^2 = 0.27$, $p = 0.01$). Dashed lines represent 95% confidence interval. The results show that, for 4 Antarctic ice cores, there is strong evidence for Antarctic temperature in phase with northern hemisphere insolation on orbital timescales.

https://doi.org/10.1038/s41561-022-01095-x

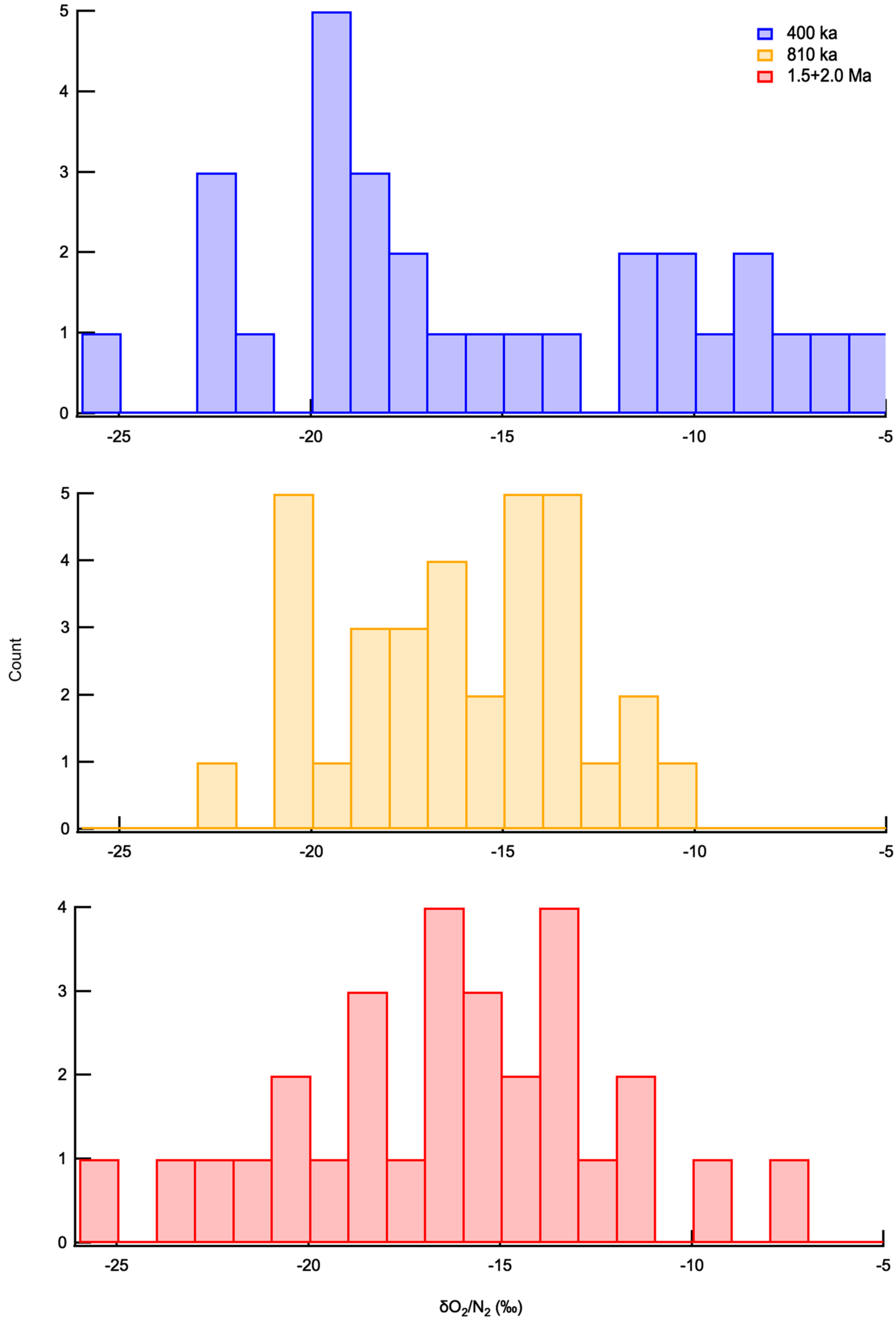

Extended Data Fig. 7 | Distribution of δO_2/N_2 measured in Allan Hills ice core samples. Because the range of the data in late- and early-Pleistocene samples is similar, the observed negative correlation between δO_2/N_2 and δD_{ice} in 1.5 and 2.0 Ma ice samples is unlikely to be the result of ice samples covering an obliquity-dominant insolation cycle. Histogram bin size is 1‰.

https://doi.org/10.1038/s41561-022-01095-x

Extended Data Table 1 | Summary of δO_2/N_2 and δAr/N_2 data used in this study

Ice core name	References	Data age range	Gas preserved as …	When was the standard air collected?	δAr/N_2 included?
ALHIC1502 and 1503	Yan et al.[20,31]	Four "snapshots": ~400 ka, ~800 ka, ~1.5 Ma, and ~2.0 Ma	Bubbles only	1990	Yes
S27	Yan et al.[30]	115-234 ka[*]	Bubbles only	1990	Yes
Vostok	Bender[29]	6-434 ka	Bubbles + clathrates	1990	No
Dome Fuji	Kawamura et al.[16]	82-325 ka	Clathrates only	1999	No
Dome Fuji	Oyabu et al.[28]	3-173 ka	Bubbles + clathrates	2017	Yes
Dome C	Landais et al.[25]	102-801 ka	Clathrates only	2005-2008[†]	No
Dome C	Bazin et al.[18]	102-801 ka	Clathrates only	2012-2013[†]	No
Dome C	Extier et al.[26]	163-332 ka	Clathrates only	2016	No
Dome C	Haeberli et al.[27]	1-700 ka	Bubbles + clathrates	2016.6	Yes

* S27 samples younger than 119 ka and older than 144 ka are excluded.

† Data measured by Landais et al.[25] and Bazin et al.[18] are not distinguishable. As a result, we treat the collection year as 2009, which introduces an error up to ±0.08‰ in the δO_2/N_2 record.